Chinese Chemical Letters 33 (2022) 2715–2720

Contents lists available at ScienceDirect

Chinese Chemical Letters

journal homepage: www.elsevier.com/locate/cclet

# Hybrid supraparticles of carbon dots/porphyrin for multifunctional tongue-mimic sensors

Rong Hu[a], Xingchun Zhai[a], Yubin Ding[b], Guoyue Shi[a], Min Zhang[a,*]

[a] School of Chemistry and Molecular Engineering, Shanghai Key Laboratory for Urban Ecological Processes and Eco-Restoration, Shanghai Key Laboratory of Multidimensional Information Processing, Engineering Research Centre for Nanophotonics and Advanced Instrument (Ministry of Education), East China Normal University, Shanghai 200241, China

[b] Department of Chemistry, College of Sciences, Nanjing Agricultural University, Nanjing 210095, China

ARTICLE INFO

*Article history:*
Received 6 July 2021
Revised 31 July 2021
Accepted 24 August 2021
Available online 28 August 2021

*Keywords:*
Supraparticles
Carbon dots
Porphyrin
Pattern recognition sensor array
Heavy metal ions
Thiols

ABSTRACT

Supraparticles (SPs), such as assembly of inorganic components with organic, have made tremendous attention in biochemical analysis, which represents a novel but challenging research orientation. Herein, a single-SPs multifunctional fluorescent sensor array has been developed for high-throughput detection of heavy metal ions in biofluids, which is based on an inorganic/organic hybrid SPs consisting of carbon dots (CDs) and an easily available porphyrin [5,10,15,20-tetra(4-carboxyphenyl)porphyrin (TCPP)]. TCPP can aggregate with the CDs to form the assembly (CDs/TCPP SPs) through the electrostatic and $\pi$-$\pi$ stacking interaction. There are two independent and clearly separated fluorescence emission peaks at 470 and 668 nm in the resultant CDs/TCPP SPs under 380 nm excitation. As a proof-of concept design, $F_{470}$, $F_{668}$, $F_{668}/F_{470}$ of SPs are chosen as three sensor components to constitute our sensor array. With the addition of metal ions, three sensor components can generate different fluorescence response patterns for discriminating 11 heavy metal ions *via* principal component analysis (PCA). Additionally, thiols can readily capture $Cu^{2+}$ to switch the fluorescence of CDs/TCPP initially altered by $Cu^{2+}$. Hence, CDs/TCPP-$Cu^{2+}$ ensemble is further demonstrated to be a powerful sensor array for pattern recognition of 7 thiols and even chiral recognition of cysteine enantiomers. This novel strategy avoids the tanglesome synthesis of multiple sensing probes and dedicates an innovative method for the facile establishment of tongue-mimic sensors, which would prospectively sprout more homologous assumptions to broaden its application toward more biosensing fields.



Supraparticles (SPs) are well known as useful nanostructures aggregated by many nanoscale units, whose self-limiting evolution relies on a quasi-equilibrium state between the attractive and repulsive forces of its ingredients [1,2]. The unique architectures and versatility of components, and ability to integrate other units have made SPs promising conduits for potential applications in various fields, such as protein stabilization, drug delivery and catalysis [3–7]. Furthermore, the marriage of inorganic components with others is arguably a prospective strategy in materials science, as there are opportunities to gain new well-defined SPs with interesting properties in a facile manner [8]. Plenty of inorganic nanoparticles can assemble to generate SPs, nevertheless, carbon-based nanocomponents are not, as carbon dots, which may be due to the small mass of carbon atoms and thus relatively weak van der Waals attractions in contrast to other materials [1].

In effect, carbon dots (CDs), acknowledged as a crucial fluorescent nanomaterial, have garnered broad scientific attention since initially perceived in 2004 [9]. By virtue of abundance hydrophilic groups, CDs possess wonderful water dispersibility and are favorable to surface functionalization. In addition, CDs own a series of excellent characteristics such as facile synthetic routes, lower cytotoxicity and excellent optical properties. These admirable properties have determined their versatile applications, ranging from biosensing, imaging and photocatalysis to biomedical diagnosis and drug delivery [10–16]. These unique properties are desired in many nanoscale assemblies being converted into practical use, rendering CDs almost ideal components for establishment of SPs-based optical sensors. In attempts to polymerize CDs into SPs, researchers have proposed many strategies such as affording backbones or bridges. For example, Sidhu *et al.* have presented a simple ratiometric fluorescence assembly system for cysteine determination in which gold nanoparticles serve as solid carrier for both CDs and $L_1$ fluorophore units [17]. Also, Hao *et al.* have developed

* Corresponding author.
*E-mail address:* mzhang@chem.ecnu.edu.cn (M. Zhang).

https://doi.org/10.1016/j.cclet.2021.08.110
1001-8417/

a novel fluorescent nanosensor through encapsulating CDs into Eu-2,6-pyridinedicarboxylic acid (DPA) metal organic frameworks (MOFs) for the detection of $Cu^{2+}$ with good selectivity [18]. However, there are few reports on inorganic/organic hybrid SPs formed by CDs and organic constituents. The incorporation can integrate the superiorities of organic and inorganic components in a valid manner. Given this, it is highly desired for simple and multiplex CDs-based inorganic/organic SPs to realize accurate and effective identification.

Fluorescence-based sensors have gained tremendous popularity with their merits of quick response, low detection limits, technical simplicity and non-invasiveness [19,20]. Nevertheless, conventional fluorescence sensors demand a receptor with high specificity to analyte, namely "lock and key" sensing mode, making them virtually impossible to identify diverse analytes. Taking this issue into account, a "chemical nose/tongue" strategy based on sensor array could be introduced to achieve high-throughput determination and pattern identification of multiple targets [21]. For this strategy, different analytes produce distinctive responses which can be easily captured and applied to distinguish analytes. This approach has emerged as a potential alternative to conventional methods for the identification of metal ions, amino acids and proteins [22–25]. Despite having progress, these sensor arrays are subject to drawbacks such as complex synthesis of materials, sophisticated preparation of multiple sensing units and lack of application in biofluids. Therefore, it has definitely realistic significance to construct a facile, sensitive and reliable pattern identification approach based on SPs composing of CDs and organic substance for the discrimination of multiple targets in biofluids.

Due to the non-degradable property, heavy metals will access to the human body along the food chain and eventually accumulate in the living organisms, which will cause serious issues for human health [26]. Typically, as a fundamental trace metal element for human beings, Cu devotes its great effort to biological process of catalyzing, maintaining a normal nervous system and assisting hematopoietic function [27]. A metabolism disorder and pathological unbalance of Cu will result in the occurrence and development of Wilson's disease and other neurodegenerative disorders such as Alzheimer's disease and Parkinson's disease [28]. Thiols, which are widely distributed in living bodies, act as a significant role in maintaining the normal of life activities. Generally, the abnormal level of thiols has been reported to be associated with several illnesses, for instances, psoriasis, liver damage, leucocyte loss and cancer [29].

Inspired by the above facts, we herein construct novel single-SPs fluorescence sensing platforms based on carbon dots/porphyrin [5,10,15,20-tetra(4-carboxyphenyl)porphyrin] supraparticles (CDs/TCPP SPs) to versatilely recognize various heavy metal ions and thiols (Scheme 1). The positively charged CDs were prepared by one-step hydrothermal carbonization method, in which polyethyleneimine (PEI) and folic acid (FA) were used as passivation reagent and carbon source respectively [30]. Then, CD and TCPP were assembled to formulate CDs/TCPP SPs where weak van der Waals forces (vdW) were increased by electrostatic interaction and $\pi$-$\pi$ stacking interplay. In fact, TCPP serves here as a crosslinker-like component in the SPs architecture as well as a partial fluorescent source for the entire probe. Remarkably, these SPs realize a combination of both fluorescent properties and different peak-positions are likely to generate a distinctive fluorescence alteration, which are appropriate for pattern recognition. Thus, our sensor array is comprised of $F_{470}$, $F_{668}$ and $F_{668}/F_{470}$ of SPs. In this work, 11 heavy metal ions ($Cu^{2+}$, $Hg^{2+}$, $Cd^{2+}$, $Pb^{2+}$, $Co^{2+}$, $Ni^{2+}$, $Mn^{2+}$, $Cr^{3+}$, $Zn^{2+}$, $Fe^{3+}$ and $Fe^{2+}$) were employed as the analytes. Owing to the diverse interaction between heavy metal ions and SPs, 11 kinds of metal ions perform various fluorescence responses, which can be further analyzed by principal component analysis (PCA). Furthermore, our tongue-mimic sensor array can realize the identification of metal ions in complex biological environments, such as urine and saliva, promising its practical application. Meanwhile, the detection of 7 kinds of thiols can be achieved by utilizing another designed CDs/TCPP-$Cu^{2+}$ sensor array because thiols can powerfully affect the fluorescence signal of CDs/TCPP-$Cu^{2+}$.

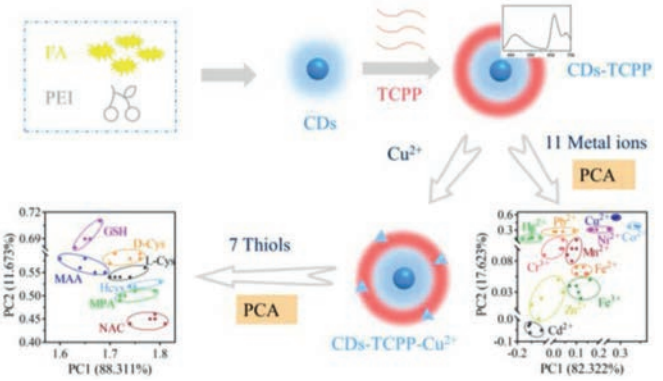


**Scheme 1.** SPs-based sensor arrays for pattern discrimination of metal ions and thiols.

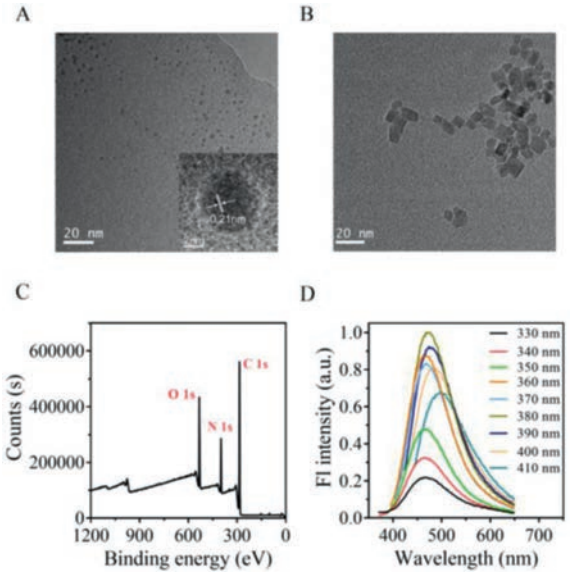


**Fig. 1.** The characterization of CDs. (A, B) TEM image of CDs and CDs/TCPP SPs, inset was its HRTEM image. (C) the XPS spectrum of CDs and (D) fluorescence spectra of the CDs solution at different excitation wavelengths.

FA was selected as the carbon source and PEI as the nitrogen source for the synthesis of CDs under hydrothermal conditions. The size and morphology of bare CDs were characterized by transmission electron microscopy (TEM). As shown in Fig. 1A and Fig. S1 (Supporting information), the obtained CDs display high polydispersity with the size distribution of 1.4-4.6 nm in diameter. The high-resolution TEM image (Fig. 1A, inset) shows a well-resolved lattice structure with an interlayer spacing of 0.21 nm which is consistent with the (100) diffraction facet of graphite carbon [31].

The surface groups and composition chemistry of CDs were investigated by Fourier transform infrared (FT-IR) spectra and X-ray photoelectron spectroscopy (XPS) analysis. As exhibited in Fig. S2 (Supporting information), the stretching vibration peaks of O–H/N–H groups (3270 $cm^{-1}$), C=O (1602 $cm^{-1}$) and C–O (1286 $cm^{-1}$) reveal the presence of amino, carboxyl and hydroxyl groups in the CDs. Moreover, absorption peaks at 2800-3000 $cm^{-1}$, 1578 $cm^{-1}$, 1456 $cm^{-1}$ and 1378 $cm^{-1}$ are in accord with $\upsilon$(C-H), $\upsilon$(C=C),

$\delta$(C–H) and $\upsilon$(C–N), suggesting that our CDs are attached with nitrogen-rich groups and aromatic structure. From XPS results, three main peaks center at 284.8, 398.3 and 531.9 eV, which are attributed to C 1s, N 1s and O 1s with atomic occupancies of 69.68%, 14.06% and 16.26% (Fig. 1C). The high-resolution spectrum of C 1s exhibits three peaks at 287.7, 286.2, 284.8 eV, corresponding to the binding energy of C=O, C–N/C–O and C=C/C–C (Fig. S3 in Supporting information). Furthermore, the high-resolution O 1s spectrum is well deconvoluted into two peaks of 532.6 and 530.6 eV, which can be related to C=O and C–O, further verifying the existence of carboxyl and hydroxyl groups in CDs (Fig. S3). Thus, the surface structure information obtained by XPS is in good agreement with the FTIR results, reflecting plenty hydrophilic units such as amino and carboxyl groups upon the CDs.

To elucidate the distinct optical property of CDs, we carried out fluorescence and ultraviolet−visible (UV-vis) absorption experiments and the spectra were illustrated in Fig. 1D and Fig. S4 (Supporting information). Specifically, as excitation wavelength varies from 330 to 410 nm, fluorescence peaks undergo gradual wavelength shifts which summarize as the excitation-dependent emission behavior. The maximum emission intensity appears at around 470 nm under the excitation of 380 nm, so 380 nm is chosen as the optimal excitation in the following experiments. Additionally, two distinct absorption peaks can be observed at 284 nm and 364 nm in the UV-vis spectrum of CDs (Fig. S4). The absorption peak at 284 nm may derive from $\pi$-$\pi^*$ transition of rich aromatic chromophores, while another one located at 364 nm is attributed to the n−$\pi^*$ transition of CDs.

Porphyrins, the dyestuffs of the world, are a sort of heterocyclic macrocyclic compounds with inherent optical characteristics and abundant coordination sites; thus, they are possibly appropriate as candidates for the development of CDs SPs-based sensors [32]. TCPP, a water-soluble and commercially available porphyrin compound, has various affinities with different analytes via their characteristic structures, making it a model component to construct our sensor array. TCPP has four carboxyl groups, which can coordinate with the positively charged CDs in certain alkaline solution environments. The negative charge of TCPP at pH 7.4 is not as strong as that at pH 8.5, and thus binding to positively charged CDs becomes more difficult, which is not conducive to SPs formation and subsequent pattern recognition assay (Fig. S5 in Supporting information). In this respect, we tentatively employed buffer solution at pH 8.5 to realize the assembly process for subsequent experiments. In order to prove the successful combination of CDs and TCPP, we studied zeta potential of CDs, TCPP and CDs/TCPP. Zeta potentials of CDs, TCPP and CDs/TCPP are +24.0, −39.1 and +11.0 mV, respectively (Fig. S6 in Supporting information). The absorption spectra of CDs, TCPP and CDs/TCPP SPs were exhibited in Fig. S4. It is worth noting that the absorption characteristics of the two components merge together in the SPs, further demonstrating that the CDs have gathered to become inorganic/organic SPs as expected. Moreover, the TEM of CDs/TCPP also shows a larger particle size compared with the CDs alone (Fig. 1B). In short, the above results declare successful aggregation of CDs and TCPP to form SPs.

In order to concretely evaluate the possibility of CDs/TCPP SPs as a single signal source for multiple metal ions, the spectrum experiments were initially conducted. The fluorescence spectra of CDs/TCPP and CDs/TCPP-$Cu^{2+}$ excited at 380 nm were determined and the results were shown in Fig. 2A. Compared with CDs and TCPP alone (Fig. S7 in Supporting information), CDs/TCPP SPs display fluorescent emissions at 470 and 668 nm, indicating that the SPs have been equipped with fluorescence characteristics of both. Especially, the emission peaks are obviously separated, which may become beneficial to evaluate fluorescent answers with great accuracy for the subsequent assay. With the import of $Cu^{2+}$ to CDs/TCPP, fluorescence intensity at 470 nm slightly decreases while

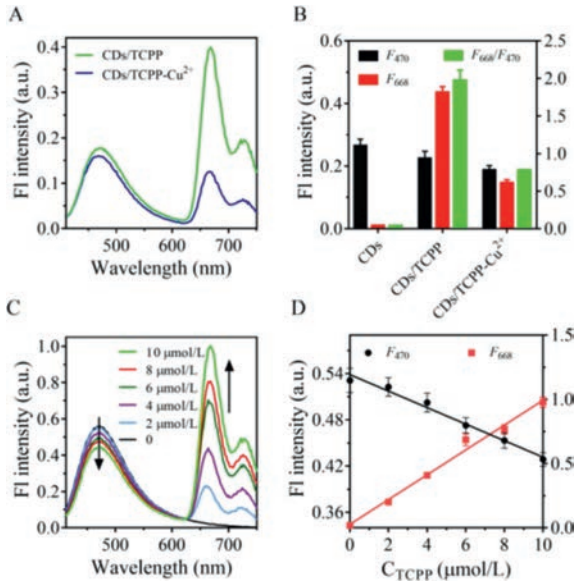


**Fig. 2.** (A) Fluorescence spectra of CDs/TCPP and CDs/TCPP-$Cu^{2+}$; (B) the histogram of $F_{470}$, $F_{668}$ and $F_{668}/F_{470}$ corresponding to the fluorescence spectrum; (C) fluorescence spectra of CDs/TCPP at different TCPP concentrations; (D) the relationship of $F_{470}$ and $F_{668}$ with the concentration of TCPP.

the intensity at 668 nm significantly reduces (Fig. 2A). The quenching levels of $F_{470}$, $F_{668}$ and $F_{668}/F_{470}$ are different, which makes it possible to construct a sensor array for metal ions (Fig. 2B). Thereafter, $F_{470}$, $F_{668}$ and $F_{668}/F_{470}$ with varying responses are chosen as optimal sensing elements to make up our sensor array for straightforward data capturing from the same signal source. Then, we optimized the concentration of CDs and TCPP for the preparation of CDs/TCPP SPs to improve its sensitivity. Different concentrations of TCPP were mixed with CDs at a constant concentration (0.2 mg/mL). As depicted in Figs. 2C and D, with the concentration of TCPP varying from 0 to 10 μmol/L, the fluorescence intensity of CDs/TCPP at 668 nm gradually increases while the emission at 470 nm reduces, which would result in a corresponding enhancement of $F_{668}/F_{470}$. This reduction may be due to photo-induced electron transfer rather than fluorescence resonance energy transfer, because the fluorescence lifetime of 470 nm is invariable with the addition of TCPP (Fig. S8 in Supporting information). This platform is designed to realize that CDs/TCPP SPs can be excited by a single wavelength for differentiation of metal ions. Consequently, the fluorescence intensity at 470 and 668 nm should not be extremely different, which can be satisfied as the concentration is 10 μmol/L. Hence, 10 μmol/L was selected as the optimal concentration of TCPP toward 0.2 mg/mL CDs for the construct of CDs/TCPP sensor array.

We tested the fluorescent response of each sensor element of CDs/TCPP (*i.e.,* $F_{470}$, $F_{668}$, $F_{668}/F_{470}$) towards different metal ions. The resultant fluorescence responses were gathered for producing ultimate pattern data ($1\text{-}F/F_0$) and corresponding heat map. From Figs. 3A and B and Fig. S9 (Supporting information), distinct recognition patterns towards metal ions can be intuitively observed, implying that the raised sensor array could generate cross-reactive responses to metal ions and may distinguish metal ions. For $Cu^{2+}$, the dramatic attenuation of fluorescence signal at 668 nm is ascribed to intimate interplay between TCPP and $Cu^{2+}$, which will be discussed in detail below. To further comprehend fluorescence pattern of the SPs array towards different target metals, principal component analysis (PCA) was performed to cut down the dimension of the data and concentrate the most prominent features. In our test, the two-dimensional (2D) PCA graphs were derived

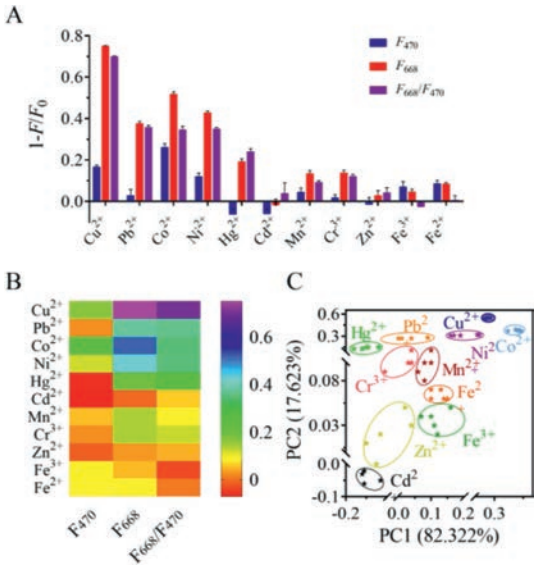


**Fig. 3.** Discrimination of multiple metal ions. (A) Fluorescence response patterns of CDs/TCPP SPs sensor array toward 11 metal ions. (B) Heat maps derived from the fluorescence response patterns. (C) PCA plot for fluorescence response patterns obtained with CDs/TCPP sensor array.

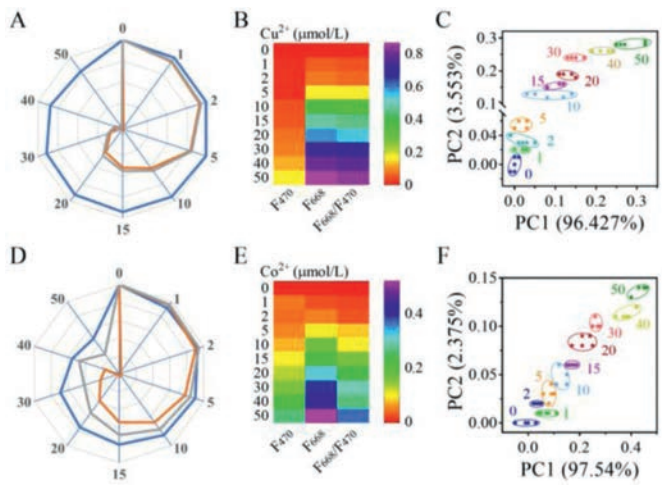


**Fig. 4.** Identification of $Cu^{2+}$ and $Co^{2+}$ at different concentrations. (A, D) The radar maps from the fluorescence changes ($1\text{-}F/F_0$) based on pattern recognition of metal ions. (B, E) Heat maps derived from the fluorescence response patterns. (C, F) PCA plots for the detection of $Cu^{2+}$ and $Co^{2+}$ in different concentrations. The blue, orange and gray lines correspond to $F_{470}$, $F_{668}$ and $F_{668}/F_{470}$ respectively in radar maps.

from the two most significant typical factors, where each point represented a single signal of particular metal ion to proposed SPs sensor array. As shown in Fig. 3C, resulting PCA map attests the discriminating ability of the system by generating 11 well-divided clusters for metal ions (50 μmol/L). Due to the presence of nitrogen-rich and oxygen-rich groups in SPs, it is rational to assume that different metal ions can influence emission intensity of CDs/TCPP with varying degrees to produce various signals. In order to make this method more suitable for practical applications, we also tested metal ions at a lower concentration (10 μmol/L) using CDs/TCPP sensor array (Fig. S10 in Supporting information). Likewise, Fig. S10C shows that metal ions at a lower concentration follow certain patterns and can be well-separated into 11 groups. Given the fact that it is a rapid detection of low concentrations of metal ions, it can be assumed that precipitate issue has little effect on the pattern recognition.

After successful identification of metal ions, it is imperative to evaluate the sensitivity of CDs/TCPP sensor array toward particular metal ion with various concentrations. Hence, we chose $Cu^{2+}$ and $Co^{2+}$ as typical analytes, which played a vital role in the biological system. Many diseases are attributed to unusual levels of these heavy metal ions, such as Alzheimer's disease [33]. In this work, we used the sensor array to recognize $Cu^{2+}$ and $Co^{2+}$ with different concentrations, respectively (Fig. 4 and Fig. S11 in Supporting information). It can be seen from Figs. 4A and D that as the concentration increases, the quenching rates of $F_{470}$, $F_{668}$ and $F_{668}/F_{470}$ are variant. The signal differences of multiple analytes with the sensor array can be visually represented as a heat map as Figs. 4B and E, which both show a gradual colorific change in tendency. Meanwhile, the PCA diagrams possess a certain rule that data points of the same concentration are clustered close together and the various are obviously isolated from each other without overlap (Figs. 4C and F). Because PC2 is less than 40%, it is also reasonable to apply PC1 to achieve the quantification of metal ions. Next, we fitted the correlation linear curve of ion concentration and PC1 value and the relative coefficients ($R^2$) reached 0.9821 and 0.9824 (Fig. S11). The limits of detection for $Co^{2+}$ and $Cu^{2+}$ were 0.90 and 1.16 μmol/L. According to the above experimental results, CDs/TCPP can achieve semi-quantitative pattern recognition of metal ions through concentration-dependent changes of output signals.

To further understand the quenching mechanism of sensor array, the fluorescence decay curves of CDs/TCPP in the absence and presence of $Cu^{2+}$ were studied and shown in Fig. S8. With the addition of $Cu^{2+}$, the fluorescence lifetime at 668 nm of CDs/TCPP decreases from 9.815 ns to 3.895 ns, demonstrating that dynamic quenching between CDs/TCPP and $Cu^{2+}$ occurs. On the other hand, due to the formation of a non-fluorescent complex, $Cu^{2+}$ also has a static quenching effect on CDs/TCPP (Fig. S12 in Supporting information). According to the Stern–Volmer equation, if fluorescence quench mechanism is dynamic quenching, the fluorescence intensity and lifetime are subjected to an equally proportional reduction in the presence of the quencher ($F_0/F = \tau_0/\tau$). For the static quenching, the fluorescence intensity gradually decreases with increasing concentration of the quencher, while the lifetime remains constant. Herein, once $Cu^{2+}$ is introduced, the diminutions in fluorescence intensity and lifetime appear simultaneously, but do not abide by an equal proportion, further revealing that dynamic and static quenching exist both. Furthermore, the value of $F_0/F$ is more than $\tau_0/\tau$, which confirms that the dominant factor is static quenching in the quenching mechanism.

Since having proved an excellent distinguishability of CDs/TCPP toward metal ions with different contents, the next challenge is to investigate its discrimination performance toward coexisting metal ions. We took $Cu^{2+}/Co^{2+}$ and $Cu^{2+}/Ni^{2+}$ = 50/0, 40/10, 30/20, 25/25, 20/30, 10/40 and 0/50 μmol/L mixture as analytes to demonstrate the recognition ability of CDs/TCPP sensing system toward the mixtures (Fig. S13 in Supporting information). In respect of the mixtures of $Cu^{2+}/Co^{2+}$ with different molar ratios, fluorescence signals are diverse and fluorescence response patterns are visibly discrete in PCA results (Figs. S13A and B). The same consequence can be obtained in the samples of $Cu^{2+}/Ni^{2+}$ that each molar ratio displays a unique fluorescence response, which enables them reliably discerned in the PCA map (Figs. S13C and D). The above results clearly indicate that the sensing system can successfully identify metal ion mixtures with accuracy.

The amount of metal ions in biofluids (including saliva and urine) can reflect valuable vital sign information, which plays an essential role in human health. For example, out-of-balance of $Cu^{2+}$ in body will lead to severe disorders, such as kidney and liver damage, gastrointestinal dysfunction, Alzheimer's disease and Wil-

**Table 1**
Detection of $Cu^{2+}$ in artificial urine using CDs/TCPP sensor array.

| Entry | Actual (μmol/L) | ICP-AES (μmol/L) | CDs/TCPP (μmol/L) | Recovery (%) | RSD[a] (%) |
|---|---|---|---|---|---|
| Urine | 5 | 4.92 | 5.37 | 107.4 | 2.35 |
| | 10 | 10.23 | 10.53 | 105.3 | 1.38 |
| | 15 | 15.28 | 14.72 | 98.1 | 1.67 |

[a] Relative standard deviation.

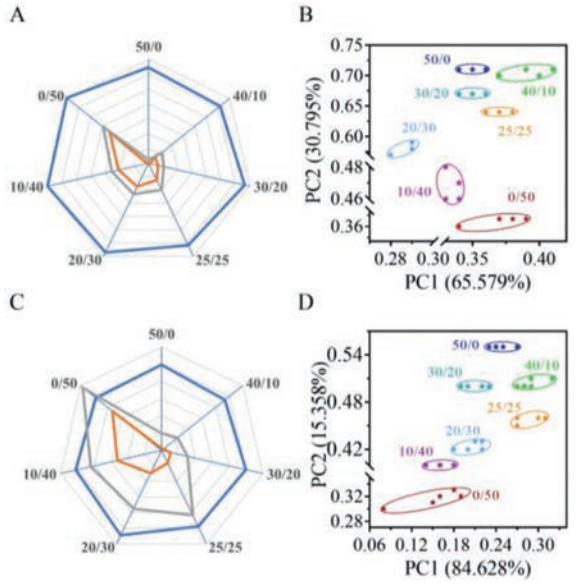


**Fig. 5.** Differentiation of mixed samples in artificial urine and saliva. (A, C) The radar map from the fluorescence changes (1-$F/F_0$) and (B, D) PCA plots of CDs/TCPP sensor array toward the mixtures of $Cu^{2+}/Co^{2+}$ and $Cu^{2+}/Ni^{2+}$. The blue, orange and gray lines correspond to $F_{470}$, $F_{668}$ and $F_{668}/F_{470}$ respectively in radar maps.

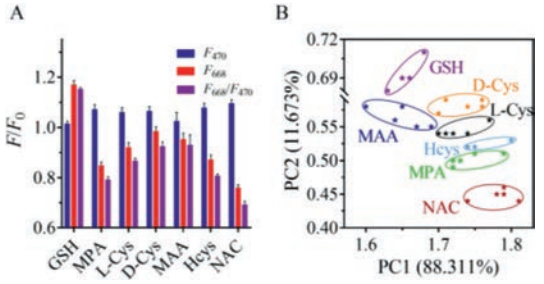


**Fig. 6.** Discrimination of multiple thiols. (A) Fluorescence response ($F/F_0$) and (B) PCA plot of CDs/TCPP-$Cu^{2+}$ sensor array toward 7 thiols.

son's Syndrome [34]. Therefore, it is of great significance to use presented CDs/TCPP to realize sensitive detection of $Cu^{2+}$ in biofluids. So, we proposed to investigate the feasibility of detecting $Cu^{2+}$ in artificial urine and saliva using this sensor array. As illustrated in Table 1 and Table S1 (Supporting information), the recovery rates of $Cu^{2+}$ in artificial urine fluctuate from 98.1% to 107.4%, while that in saliva vary from 93.2% to 102.1%. The concentration of $Cu^{2+}$ obtained from recovery experiments is well consistent with the results acquired by traditional inductively coupled plasma-atomic emission spectrometry (ICP-AES) method, indicating that CDs/TCPP sensor array has potential applications for detecting metal ions in complex environments and preliminarily diagnosing diseases correlated with an abnormal metal concentration in biofluids.

To assess the potential of our sensor array to recognize the mixture of metal ions in biofluids, several liquid hybrids were prepared in artificial urine and saliva. We chose $Cu^{2+}/Co^{2+}$ and $Cu^{2+}/Ni^{2+}$ mixtures to explore the sensing ability of CDs/TCPP toward biofluid-related mixtures. A series of mixture groups comprised of $Cu^{2+}/Co^{2+}$ and $Cu^{2+}/Ni^{2+}$ at distinct mole ratios (50/0, 40/10, 30/20, 25/25, 20/30, 10/40, and 0/50, all in μmol/L) were injected into artificial urine and saliva. It can be seen from the radar maps (Figs. 5A and C) that fluorescence intensity of mixed samples with different ratios is no significant difference, but differences always exist, which renders them distinguishable from each other. From the PCA plots for the fluorescence response in the biological liquids, our CDs/TCPP sensing system has a powerful ability to assign these mixed samples into several clusters (Figs. 5B and D). These results indicate that the sensor array is equipped with an excellent resolution capability for mixed samples of metal ions in complex environments.

Except for recognizing metal ions, CDs/TCPP can combine with $Cu^{2+}$ to form another assembly (CDs/TCPP-$Cu^{2+}$) toward detecting thiols, because thiols have a strong binding tendency with $Cu^{2+}$ to change the fluorescence of CDs/TCPP previously influenced by $Cu^{2+}$. As a proof of concept, 7 thiols, including reduced glutathione (GSH), 3-mercaptopropionic acid (MPA), L-cysteine (L-Cys), D-cysteine (D-Cys), mercaptoacetic acid (MAA), homocysteine (Hcys) and *N-acetylcysteine* (NAC), were selected as experimental samples for evaluating identification ability of our CDs/TCPP-$Cu^{2+}$ sensor array. From Fig. 6A, it is apparent that each thiol can generate distinct fluorescent feedback, which implies the feasibility of applying our CDs/TCPP-$Cu^{2+}$ sensor array to discriminate these thiols. Then, converting these fluorescent signals into a PCA plot by lowering the data dimensionality. It can be seen from Fig. 6B that each thiol can be gathered in a certain range and isolated from other thiols. These results provide intuitive evidence for the effective identification of different thiols utilizing CDs/TCPP-$Cu^{2+}$ sensor array.

GSH with various concentrations was chosen as the analyte to prove the sensitivity of CDs/TCPP-$Cu^{2+}$ sensor array toward thiol. As shown in Fig. S14A (Supporting information), for each concentration of GSH, the fluorescence response displays a fingerprint-like difference. Moreover, owing to the subtle changes, various concentrations of the same metal ion are obviously separated in the PCA plot (Fig. S14B in Supporting information). Chirality is a significant characteristic in biological phenomena. Enantiomeric recognition of chiral compounds is essential in process development and quality control. Mixtures of L-Cys and D-Cys with different molar ratio (100/0, 80/20, 60/40, 50/50, 40/60, 20/80 and 0/100, all in μmol/L) were further investigated with CDs/TCPP-$Cu^{2+}$ sensory system. As exhibited in Figs. S14C and D (Supporting information), the fluorescence answers from CDs/TCPP-$Cu^{2+}$ are diverse and now-available cases are classified into many bunches in the 2D PCA graph, which indicates that the sensor array has a good discrimination competence toward chiral molecules with different molar ratios. Hence, CDs/TCPP-$Cu^{2+}$ sensor array has broad application prospects because it can realize pattern identification for different concentrations of thiols and chiral cysteine enantiomers with good accuracy.

In conclusion, we have developed effective sensor arrays based on CDs/TCPP SPs for high-throughput detection and pattern recognition of metal ions and thiols. TCPP was assembled onto the CDs to form CDs/TCPP SPs *via* electrostatic and $\pi$-$\pi$ stacking interactions. $F_{470}$, $F_{668}$, $F_{668}/F_{470}$ of CDs/TCPP were innovatively chosen

as three sensor components to constitute our sensor array. By being challenged with different metal ions, the three sensor components can generate different fluorescence response patterns for discriminating 11 heavy metal ions *via* principal component analysis (PCA). Moreover, different concentrations of the same metal ions and metal ions mixtures are able to get distinguished in buffer and biofluids, promising its potential toward the non-invasive diagnosis of metal ion-reverent diseases. Since thiols can readily remove $Cu^{2+}$ to tune the fluorescence of CDs/TCPP initially altered by $Cu^{2+}$, we further demonstrated that the ensemble of CDs/TCPP-$Cu^{2+}$ can be an appealing sensor array for pattern recognition of 7 thiols and even chiral recognition of cysteine enantiomers. The present study will broaden the scope of tongue-mimic research and inspire more development of single-element multifunctional sensing platforms.

## Declaration of competing interest

The authors declare that they have no known competing financial interests or personal relationships that could have appeared to influence the work reported in this paper.

## Acknowledgments

This work was supported by the National Natural Science Foundation of China (No. 21775044), the Shanghai Science and Technology Committee (Nos. 19ZR1473300, 18DZ1112700), the Shanghai Key Laboratory of Multidimensional Information Processing (No. MIP202104), and the Fundamental Research Funds for the Central Universities.

## Supplementary materials

Supplementary material associated with this article can be found, in the online version, at doi:10.1016/j.cclet.2021.08.110.

## References

[1] Z.B. Qu, X. Zhou, M. Zhang, et al., Adv. Mater. 23 (2021) e2007900.
[2] S. Wintzheimer, T. Granath, M. Oppmann, et al., ACS Nano 12 (2018) 5093–5120.
[3] K. Zhang, J. Yi, D. Chen, J. Mater. Chem. A 1 (2013) 14649–14657.
[4] K. Niikura, N. Iyo, Y. Matsuo, H. Mitomo, K. Ijiro, ACS Appl. Mater. Interfaces 5 (2013) 3900–3907.
[5] S. Jiang, M. Chekini, Z.B. Qu, et al., J. Am. Chem. Soc. 139 (2017) 13701–13712.
[6] W. Yan, L. Xu, C. Xu, et al., J. Am. Chem. Soc. 134 (2012) 15114–15121.
[7] K. Zhu, D. Wang, J. Liu, Nano Res. 2 (2010) 1–29.
[8] T. Fenske, H.G. Korth, A. Mohr, C. Schmuck, Chemistry 18 (2012) 738–755.
[9] X. Xu, R. Ray, Y. Gu, et al., J. Am. Chem. Soc. 126 (2004) 12736–12737.
[10] Q. Su, L. Gan, Y. Zhu, X. Yang, Sens. Actuators B 335 (2021) 129715.
[11] D. Gao, A. Liu, Y. Zhang, et al., Chem. Eng. J. 415 (2021) 128984.
[12] P. Karfa, E. Roy, S. Patra, et al., RSC Adv. 5 (2015) 58141–58153.
[13] H. Li, R. Liu, Y. Liu, et al., J. Mater. Chem. 22 (2012) 17470–17475.
[14] X. Guo, C.F. Wang, Z.Y. Yu, L. Chen, S. Chen, Chem. Commun. 48 (2012) 2692–2694.
[15] M. Zheng, S. Liu, J. Li, et al., Adv. Mater. 26 (2014) 3554–3560.
[16] A.M. Alam, B.Y. Park, Z.K. Ghouri, M. Park, H.Y. Kim, Green Chem. 17 (2015) 3791–3797.
[17] J.S. Sidhu, A. Singh, N. Garg, N. Kaur, N. Singh, Sens. Actuators B 282 (2019) 515–522.
[18] J. Hao, F. Liu, N. Liu, et al., Sens. Actuators B 245 (2017) 641–647.
[19] X. Du, Y. Liu, F. Wang, et al., ACS Appl. Mater. Interfaces 13 (2021) 22361–22367.
[20] G. Singh, S.P. Pandey, P.K. Singh, Sens. Actuators B 330 (2021) 129346.
[21] J.R. Askim, M. Mahmoudi, K.S. Suslick, Chem. Soc. Rev. 42 (2013) 8649–8682.
[22] N. Cao, J. Xu, H. Zhou, et al., Microchem. J. 159 (2020) 105406.
[23] Y. Wu, X. Liu, Q. Wu, J. Yi, G. Zhang, Sens. Actuators B 246 (2017) 680–685.
[24] B. Wang, J. Han, N.M. Bojanowski, et al., ACS Sens. 3 (2018) 1562–1568.
[25] Z. Pode, R. Peri-Naor, J.M. Georgeson, et al., Nat. Nanotechnol. 12 (2017) 1161–1168.
[26] X. Hui, M. Sharifuzzaman, S. Sharma, et al., ACS Appl. Mater. Interfaces 12 (2020) 48928–48937.
[27] H. Feng, Q. Fu, W. Du, et al., ACS Nano 15 (2021) 3402–3414.
[28] O. Bandmann, K.H. Weiss, S.G. Kaler, Lancet Neurol. 14 (2015) 103–113.
[29] X. Chen, Y. Zhou, X. Peng, J. Yoon, Chem. Soc. Rev. 39 (2010) 2120–2135.
[30] X. Yang, Y. Wang, X. Shen, et al., J. Colloid Interface Sci. 492 (2017) 1–7.
[31] C. Liu, D. Lu, X. You, et al., Anal. Chim. Acta 1105 (2020) 147–154.
[32] X. Gong, T. Milic, C. Xu, J.D. Batteas, C.M. Drain, J. Am. Chem. Soc. 124 (2002) 14290–14291.
[33] Y. Shi, Q. Liu, W. Yuan, et al., ACS Appl. Mater. Interfaces 11 (2019) 430–436.
[34] L. Zeng, G. Ma, H. Xu, et al., Small 15 (2019) e1803866.